Graphitic Patterns on CVD Diamond Plate as Microheating/Thermometer Devices

Daniele Di Gioacchino,*,[†] Augusto Marcelli,[†,‡] Alessandro Puri,[†] Antonio De Sio,[‖] Mariangela Cestelli Guidi,[†] Yimamu Kamili,[⊥] Giancarlo Della Ventura,[§] Andrea Notargiacomo,[#] Paolo Postorino,[∇] Sara Mangialardo,[∇] Eckhard Woerner,[○] and Emanuele Pace[†,‖]

[†]INFN- National Laboratory of Frascati, Via Enrico Fermi 40, 00044 Roma, Italy

[‡]Rome International Center for Materials Science Superstripes, Via dei Sabelli 119A, 00185 Roma, Italy

[§]Department of Geological Science, University of Roma Tre, Largo San Leonardo Murialdo 1, 00146 Roma, Italy

[‖]University of Firenze, Physics and Astronomy Department, Largo Enrico Fermi 2, 50125 Florence, Italy

[⊥]University of Camerino, Science and Technology Faculty, Via Madonna delle Carceri 9, 62032 Camerino, Macerata, Italy

[#]IFN- Institute for Photonic and Nanotechnologies, Via Cineto Romano 32, 00156 Rome, Italy

[∇]CNR-IOM and University of Rome Sapienza, Piazzale Aldo Moro 5, 00185 Rome, Italy

[○]Diamond Materials GmbH, Hans-Bunte-Strasse 19, 79108 Freiburg, Germany

S *Supporting Information*
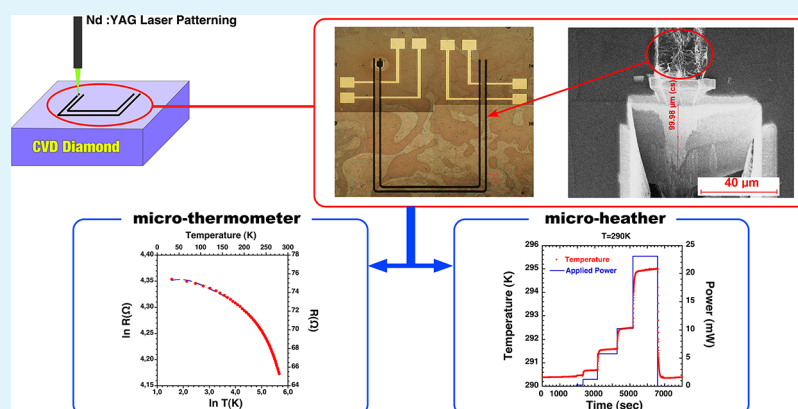
ABSTRACT: A simple compact temperature sensor and microheater in a wide temperature range has been developed, realizing a laser-patterned resistive structure on the surface of a synthetic polycrystalline diamond plate. Imaging and spectroscopy techniques used to investigate morphology, structure, and composition of the pattern showed that it incorporates different nondiamond carbon phases. Transport experiments revealed the semiconducting behavior of this microresistor. Thermal power measurements versus temperature are presented. A possible application of this device that may easily match compact experimental layouts avoiding both thermal anchoring offset and mechanical stress between sample and sensor is discussed. The patterned structure undergoes testing as a microthermometer, providing fast response and excellent stability versus time. It exhibits a good sensitivity that coupled to an easy calibration procedure minimizes errors and guarantees high accuracy. Plot of temperature versus input power of the resistive patterned line used as microheater shows a linear behavior in an extended temperature range.

KEYWORDS: CVD diamond, laser patterning, graphitic planar structure, microthermometer, microheater

INTRODUCTION

Different research areas are currently demanding optimized microheaters and microthermometers.[1] Indeed, because of the limited space available in many layouts and the increasing interest toward samples of extremely small dimensions, many applications need small devices with a fast dynamic, obviously related to size and shape of the device. Moreover, challenging thermal and electrical transport measurements have to be performed within complex experimental layouts on low-dimensional structures with extremely small areas, micro-samples (weight of a few micrograms), biological systems, cell cultures, or materials investigated under extreme conditions,

e.g., inside a diamond anvil cell (DAC).[1−4] Indeed, in a typical high-pressure experiment, a small sample is loaded inside a DAC where it may experience extreme conditions of pressure, magnetic field, and high/low temperature.[5,6] When simultaneous or concurrent experiments have to be performed on a sample inside a DAC, e.g., IR spectroscopy and AC susceptibility measurements,[7,8] the diagnostics to control the physical parameters of the experiment, such as temperature, must be reliable to fulfill ultimate requirements and be extremely compact. In fact, the temperature distribution inside a DAC cell is affected by a weak heat confinement, and a large dissipation is present.[9] This gives a large uncertainty in the temperature measurements because of the complex heat flow and to the distance of sensor(s) from the sample position.

Heaters inside a DAC for magnetic susceptibility experiments should limit heat loss to minimize thermal contributions affecting the magnetic/electric response of the sample and of other sensors set around the sample, such as SQUID superconducting magnetometers.[5,7,8] Some DAC experimental layouts allow an external laser to better control the sample heating.[4,10] In this case, drawbacks are possible because of instabilities and the occurrence of a high thermal gradient on the metallic gasket where the sample is loaded.[3,9,11] Local resistive devices are currently used as heaters. They offer good temperature stability and a quite homogeneous spatial distribution.[3] Their main disadvantage is the possible breakdown of the electric isolation while changing the pressure.[9] Samples with an adequate resistivity can be also used as heaters.[12] However, the physical properties of the analyzed sample can be affected, and a systematic error may be introduced if the heating device and the sample are too close. Because of these limitations, many experimental layouts really demand improved microthermometer and microheating devices.

To design an ultimate temperature microsensor, temperature resolution, precision, accuracy, size, stability, response time, mechanical shock resistance, interchangeability, magnetic field effects, and reliability have to be considered.[13] Diamond has unique and appealing mechanical, optical, and thermal properties, suitable for many different applications.[14] Particularly important are those associated with UV and X-ray detectors,[15−18] high-pressure experiments with diamond anvil cells (DAC),[19,20] high-energy, space, or astrophysics researches, etc. On the basis of its composition, a resistive pattern can also be fabricated on the diamond surface, although extremely accurate cleaning/deposition/lithography and microelectronic procedures have to be used in these setups.[3,9]

Because of the extremely low emissivity of diamond in the IR region, only recently has a noncontact method been developed on the basis of pyrometer devices not limited to only very high temperature (1000 K). However, the method works only for temperatures greater than 400 K.[21] In fact ,the amount of the detectable thermal radiation is low because of the small collection angle from the heated spot. Raman spectroscopy was also used, but its temperature precision (∼10 K) is not suitable for many applications.[2] Among existing temperature sensors, small thermocouples are still the simplest solution. However, a good thermal contact between the thermocouple and the diamond anvil is not easy to achieve; thus, the calibration is not reliable after many temperature cycles.[22,23]

In this work, we present and discuss the characterization of a graphitic resistive pattern fabricated on a CVD diamond plate by a laser scriber. Such a patterned device is rather low-cost, can be easily manufactured, and may be used as both temperature sensor and heating device. Moreover, it prevents failures caused by badly insulated electric contact during heating or under high-pressure applications and can be properly calibrated as a thermometer.

We characterized the morphology of the graphitic pattern using scanning electron microscopy (SEM) and focused ion beam (FIB) and studied the diamond surface in and around the patterned lines by both IR and Raman spectroscopy. Then, combining the morphological and spectroscopic information, we analyzed the different nondiamond carbon phases. Actually, we also used FIB to expose synthetic diamond in order to obtain regular patterns suitable to design complex nanodevices.[24−26]

To fully characterize the graphitic pattern as thermometer or heater, we measured the behavior of its resistance versus temperature in a wide temperature range from 4.2 to 300 K. The reproducibility of the resistance value was also assessed for different cooling and heating cycles, and its sensitivity as a temperature sensor was characterized in the same wide temperature range. Finally, to test the possible performance of the device as microheater, we also characterized the heating response of the nondiamond carbon pattern using different electric current densities that provide different applied heat powers. Actually, we chose three different temperatures in the 4.2−300 K range. Temperature versus time rate, final temperatures reached for each heating power applied, and linearity of power−temperature law are presented and discussed.

■ EXPERIMENTAL SECTION

The extreme physical properties of diamond derive from its strong, directional σ bond. Diamond has a wide 5.5 eV band gap, the largest bulk modulus among solids, the highest atom density, the largest room-temperature thermal conductivity, the smallest thermal expansion coefficient, and the largest limiting electron and hole mobility.[27] Free-standing CVD diamond samples were grown by Diamond Materials Gmbh using a microwave-plasma-CVD reactor with an ellipsoidal cavity.[28] Standard deposition conditions are a microwave power of 6 kW at a frequency of 2.45 GHz, growth temperatures between 700 and 900 °C, and pressures ranging from 100 to 200 mbar. The feeding gas mixture was 1−2% methane in hydrogen. The CVD diamond plates are 300 μm thick and have an optical-grade quality. They were grown up to 1 mm and then polished on both sides to achieve smooth surfaces and to remove the interface layer after silicon substrate removal.

The route we considered to obtain a reliable thermal sensor on CVD diamond is to produce a pattern of graphitic lines on its surface via laser irradiation. Different patterns (see Figure 1) were fabricated
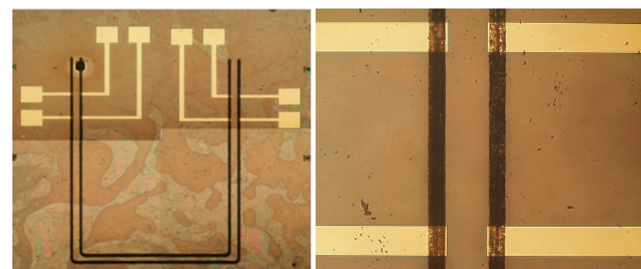

Figure 1. Left, assembled image of four optical microscope pictures showing the Au/Ag/Au contacts realized on two parallel U-shaped graphitic lines produced on the CVD diamond substrate, and right, magnified image showing details of the metallic contacts.

by Diamond Materials Gmbh on the surface of the CVD diamond layers.[29,30] The diamond crystal structure is changed when is irradiated with energetic light beams; high light energy can be delivered using a laser with high light flux of moderate energy (few electronvolt). Radiation damage is produced via thermal heating, valence ionization of carbon atoms, and deep-shell carbon atom excitation and ionization. These processes generate graphitic carbon or amorphous carbon that can sublimate or be converted into carbon compound in determinate atmospheres. It is possible obtain different diamond changing, in particular "melting" using 1−0.2 MW/mm^2 for a laser pulse duration from 20 to 100 ns or graphitization for 0.4−0.1 MW/mm^2 for pulse duration of 10−40 ns.[31] In our case, the nanosecond laser is a Q-switched Nd:YAG capable of delivering up to 2 W average power and 0.2 mJ/pulse. The energy of the laser beam on the sample is adjusted by introducing appropriate filters into the beam path. The laser is focused in a 15 μm (fwhm) focal spot size on the diamond substrate. To achieve a low resistance and to avoid the formation of carbon oxides, irradiation was performed under inert N$_2$ protective gas (99.99 purity) at 1 bar. The gas flow blew through a nozzle onto the diamond surface exactly to the point where the laser hit the diamond. Under these conditions, black lines with different shapes and line resistances of ~15 Ω/mm were obtained at room temperature.

A morphological analysis of the patterned structures (see Figure 2 and Figure 3) was performed with a dual-beam FIB (Helios Nanolab
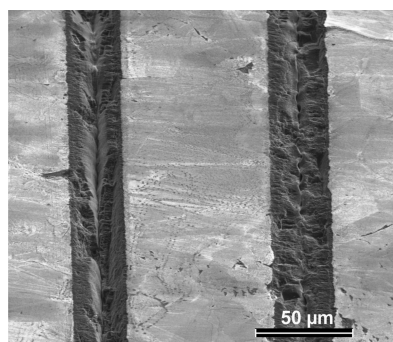

Figure 2. Magnified SEM image of graphitic patterns fabricated on a CVD diamond plate clearly showing the disordered structure of the darker regions. Scale bar is 50 μm.

600) equipped by a Ga$^+$ liquid metal ion source operated at 30 kV and a FEG-SEM column. The FIB provides unique imaging of the sample inner structure because of its capability to mill almost any material by varying ion beam parameters, including ion dose and energy, pattern shape and milling strategies, dwell time.
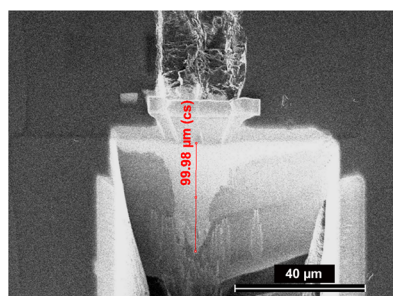

Figure 3. Section of a pattern obtained on the diamond plate. The SEM image shows the transverse milling profile of the graphitic groove. Because of the different hardness, the space filled by carbon atoms redeposited after the removal generates a brighter contrast that makes visible the geometrical profile of the vertical section of the patterned line. Vertical bar indicates the graphitic line depth that is calculated from the cross-sectional (cs) view by correcting for the tilt angle of the sample. Horizontal scale bar is 40 μm.

To characterize the properties of the structures patterned on the CVD diamond surfaces both FTIR and Raman spectroscopy were performed. These two techniques are widely used in both scientific and industrial contexts because they provide information about the bonding properties and the chemical structure of the system under investigation. When applied to investigate samples consisting of a mixture of different carbon allotropes such as graphite, diamond or amorphous carbon, they return qualitative and quantitative information about the different phases as well as their relative composition inside or at the surface of the sample. The main difference between these two analytical techniques is that IR spectroscopy detects vibrations related to changes of the electrical dipole moment, whereas Raman spectroscopy detects vibrations related to the deformation of the electrical molecular polarizability. IR spectroscopy and imaging experiments were performed at the SINBAD synchrotron IR beamline at the DAΦNE-Light laboratory (Frascati, Italy) using a BRUKER Hyperion 3000 IR-Microscope,[32] the measurements are shown in Figure 4. The two panels represent the image of the same corner area of one of the patterned groove collected with the microscope with the visible radiation, i.e., its optical density on the left, and in the right using the mid-IR radiation, The color bar indicates the IR absorption intensity integrated over the all IR range (from 600 to 4000 cm^{-1}). Blue light colors refer to lower absorption whereas orange like patterns correspond to regions of higher absorption. The measurements are given in arbitrary unit. The comparison shows clearly that the density in the infrared region is not uniform. The dark region in the left panel corresponds to the carbon groove patterned on the diamond, which absorb completely the visible light.

Raman microspectroscopy was performed at the High Pressure Spectroscopy laboratory at the University of Rome Sapienza using an optical microscope with a 50× objective, analyzing an area of ~1 μm^2 (estimated optical depth < 20 μm) with an acquisition time of 5 s per step. The spectrometer was equipped with a 20 mW He−Ne laser (632.8 nm wavelength); further details about the experimental apparatus can be found in the literature.[33] Hundreds of data points were collected along the resistive graphitic patterns at different points and along transversal directions (Figure 5).

Concerning the electric transport characterization, a four-wire contact configuration was produced on the graphitic patterns by thermal evaporation of an Au(50 nm)/Ag(300 nm)/Au(50 nm) multilayer as shown in Figure 1. The patterning of the metal contacts was made using electron beam lithography and lift-off techniques. The resistance versus temperature characteristics were measured in the LAMPS cryogenic laboratory at the Laboratori Nazionali di Frascati of the INFN, mounting the plate in a liquid-helium cryostat (4.2−300 K) with an ac sinusoidal electrical current insert using a generator with $I \approx$ 600 μA to 10 mA and f = 107 Hz.[34] The voltage response was measured with a lock-in amplifier and the temperature monitored by a DT-470 diode thermometer in good thermal contact with the patterned graphitic lines. The thermal anchorage between the thermometer and the diamond plate has been achieved with a diluted drop of varnish glue. Moreover during the measurements, a beryllium−copper spring-clip pressed the thermometer on the diamond substrate to increase the thermal contact.

To characterize the patterned lines as a thermometer, different temperature setups with variable rates, R (K/sec), within each cycle were used (see Supporting Information Figure S4). Concerning the behavior as a heater, we used a power supply operating in the range of 20 μW to 20 mW at three different temperatures: 4.2, 80, and 300 K, increasing the current from 620 μA to 20 mA. The setup of these measurements is based on a weak thermal link between the graphitic line and the heat sink that is a copper sample holder. To keep the temperature constant, the sample holder was dipped in a bath of cold He gas inside the cryostat. In these measurements, we increased the electric current value via an external electric circuit and measured the voltage of the resistive graphitic line. From the temperature variation, we calculated the corresponding dissipated power, checking simultaneously the temperature increase because of the power dissipated in the resistive graphitic line.
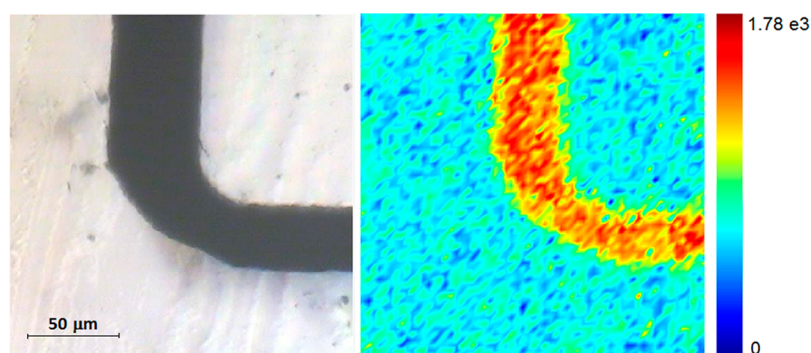
Figure 4. Comparison of (left) visible image of a pattern corner with (right) IR image. IR image was obtained by integrating the IR absorbance spectra over the whole mid-IR region (600–4000 cm^{-1}); the absorbance amplitude is given in arbitrary units. Dark blue color corresponds to the zero value, whereas orange corresponds to the maximum value.
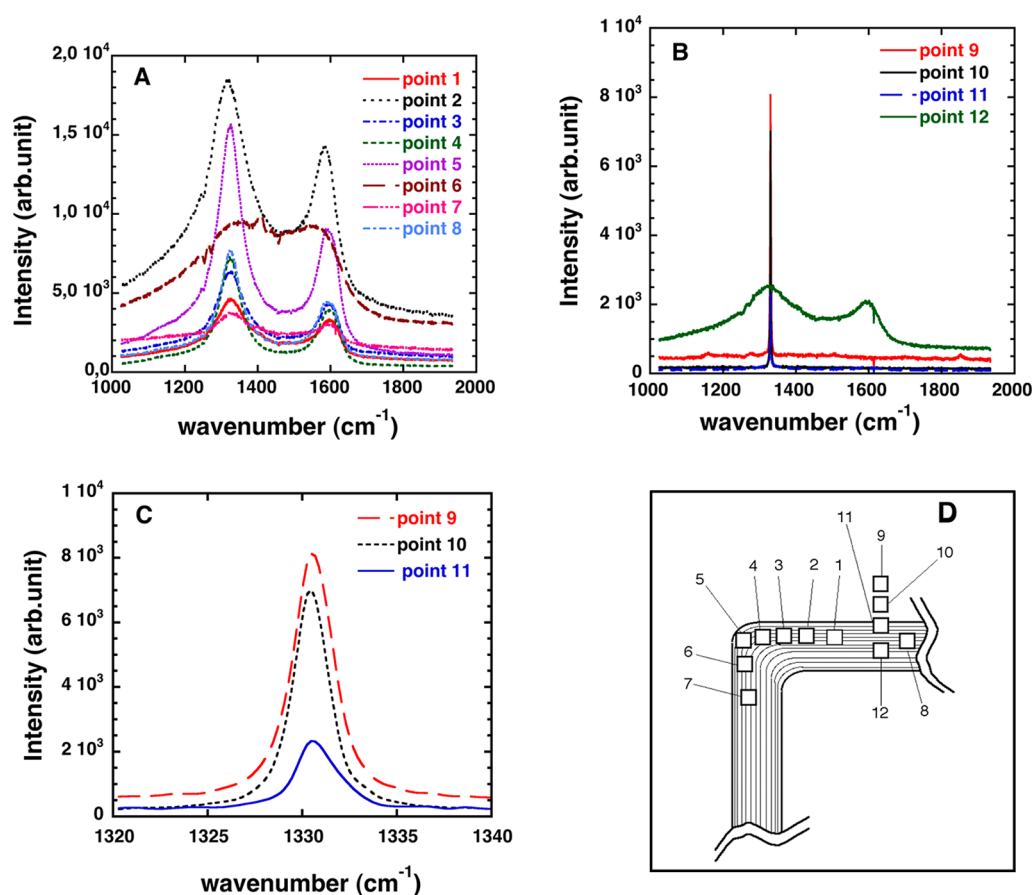

Figure 5. (A) Comparison of Raman spectra collected in the spots numbered from 1 to 8 (panel D) on the patterned line, (B) comparison of spectra collected along a line showed in the right panel starting in the non irradiated region and ending inside the pattern (from 9 to 12), (C) a magnified view of the peak of the diamond for the spectra taken at the edge of the graphitic line and three spectra taken on outside spots, and (D) points where Raman spectra have been acquired during the mapping.

RESULTS AND DISCUSSION

We show two laser-patterned graphitic lines in Figure 2. As previously mentioned in Experimental Section, the thermal load of the laser converted carbon compounds in the illuminated area on the diamond surface.[31] The resulting material is not ordered, as will be shown in the next paragraphs. Actually, the irradiation induces the amorphization of the exposed surface; the altered region may extend in depth down to ∼100 μm. As shown in Figure 2, the length of the patterned lines ranges from 6 to 12 mm, their width is ∼30 μm, and the line pitch is ∼75 μm.

Morphological Tests. The depth and shape of the section profile of the laser-annealed area were measured with the FIB technique (see Figure 3). To obtain a transversal section and to reconstruct the profile of this annealed volume, we removed layer by layer a wide region of the analyzed patterned line. The image in Figure 3 shows that the cross section is ∼30 μm wide close to the surface and has a variable vertical depth and profile. Going deeper in the bulk, the profile has a triangular shape. Actually, all images of the vertical sections show that the diamond damaging has a ∼100 μm depth. Because of the enhanced milling rate of the nondiamond carbon phase, voids

are produced during FIB milling in correspondence to the pattern. These voids are steadily filled by the redeposited material, which has an enhanced visibility in the SEM image thanks to its much brighter contrast (see Figure 3), highlighting the shape of the annealed profile. The triangular-like shape profile visible in Figure 3 resembles quite well a Gaussian profile that likely matches the (Gaussian) distribution of the intensity of the laser beam used to pattern the diamond.

Additional details of these patterned graphitic lines made on CVD diamond plates are shown in Figure 2. SEM images show additional geometrical information on the patterned lines whose morphology is clearly affected by the irradiation procedure. Large deformations and damage are induced on the diamond plate; they include the growth of columnar-ordered structures during the fast cooling process after the laser irradiation.

Spectroscopic Characterization. In addition to the morphological characterization, we examined these nonordered graphitic patterns by IR and Raman techniques to carefully identify carbon phases, bonding network, and optical properties. An IR map of a corner of one of the patterns is shown in the right panel of Figure 4. The comparison of the mid-IR image with the visible image (left panel) clearly points out that the optical properties are strongly modified only in the region that was subjected to the laser irradiation. To characterize the different properties of the irradiated and nonirradiated regions, we collected IR transmission spectra on representative points of the CVD diamond surface. Although the different absorbance between the irradiated and nonirradiated regions allows us to distinguish and map the surface easily, the direct comparison among the IR spectra is not sufficient to properly characterize the two regions. Indeed, as shown by the FIB analysis, the thickness of the irradiated layer is less than one-third of the thickness of the diamond plate (~300 μm), and for our purpose, the spatial resolution in the mid-IR region is also limited (see Figure 4). To overcome these limitations and to characterize more fully the composition and to recognize the different phases present on the diamond surface, we collected micro-Raman spectra on different spots on the patterned region.

Raman spectroscopy is a powerful and effective way to investigate the bonding structure of carbon films. The method is widely used to distinguish bonding type, domain size, and sensitivity to internal stress in amorphous and nanocrystalline carbon films.[35] We compare micro-Raman spectra of both different carbon phases and crystalline diamond in Figure 5. Spectra in the left panel (spots 1 to 8 in the map, Figure 5D) are collected in the corner region of the pattern. The spectra are characterized by the G peak related to graphite and the D peak associated with the presence of nonordered graphitic layers.[36]

Measurements were also collected along a segment from the nonirradiated regions on the diamond surface adjacent to the patterned line ending inside the irradiated graphitic line (Figure 5 B,C, points 9−12). Data in Figure 5B clearly show that the peak of diamond at 1332 cm^{-1} (points 9 and 10) decreases abruptly at the line edge, whereas a weak G peak appears. Actually, Raman spectra (see Supporting Information Figures S6−S10) nicely probe the glassy-carbon nature inside the line patterned by laser on the CVD diamond surface.

Resistance versus Temperature Measurements. For typical applications, an ideal temperature sensor has to fulfill standard characteristics such as thermal cycling reproducibility,

i.e., precision or stability, sensitivity, and accuracy,[13,37] long-term calibration drift, and appropriate dimensions to exhibit a fast response.[37] To this purpose, we measured the characteristic resistance versus temperature ($R-T$) behavior of the patterned resistor. First, the diamond plate resistance has been controlled without laser grooving; the four-point contacts technique shows a resistance greater than 100 MΩ, the measurable limit of the Agilent 34970A Data Acquisition Unit, and proves that the CVD diamond we used is a good insulator. Second, the $R-T$ curve of the patterned resistor described above was characterized in the 4.2−300 K range, using different temperature cycles (see Supporting Information Figure S4) to assess reproducibility and response. The $R-T$ experimental curves of this graphitic microresistor (see Figure 6) show high
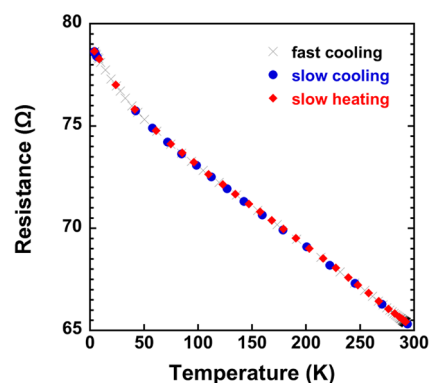
Figure 6. Comparison of the resistance vs temperature using the setup described in Figure S4. Error bars are $\Delta R \approx \pm 20$ mΩ and $\Delta T \approx \pm 10$ mK and are contained in the graphic dot size.

reproducibility. Moreover, this plot highlights a temperature-negative derivative semiconductor-like behavior, as expected from Raman spectra that show the presence of nondiamond carbon phases in the patterned line. To complete the analysis, we also show in Figure 7 a comparison between the $R-T$ characteristic curves of the patterned graphitic resistor and of commercial bulk carbon glass resistors (CGR).[38]

Concerning the resistance value in the 4.2−300 K temperature range, the resistance of the integrated graphitic line is easily measurable and shows a variation of ~13 Ω (Figure 6).
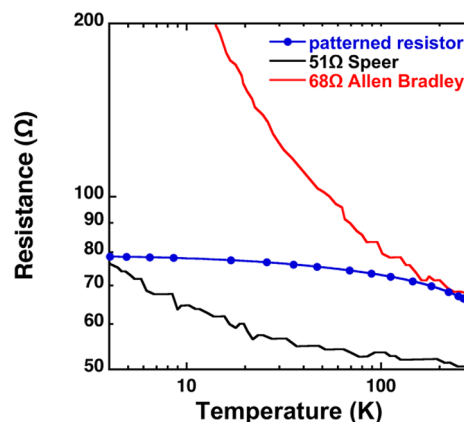
Figure 7. Comparison among $R-T$ curves of the patterned graphitic resistor and two commercial CGR thermometers with a comparable resistance at room temperature. Error bars are $\Delta R \approx \pm 20$ mΩ and $\Delta T \approx \pm 10$ mK and are contained in the graphic dot size.

Compared to the semiconductor bulk behavior of commercial CGRs, the variation shown in Figure 7 is not large but exhibits sensitivity suitable for a real device. The observed behavior, along with the results of Raman spectroscopy (see Figure 5), suggests that the different carbon phases in the graphitic lines reduce the electrical resistivity[37] (see also Supporting Information Figure S2).
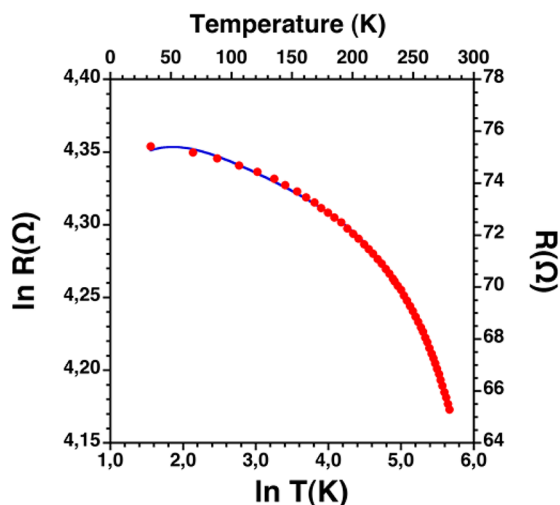

Figure 8. $R-T$ behavior of the graphitic line (red dots) fitted by eq 1 (blue line). Error bars are $\Delta R \approx \pm$ 20 mΩ and $\Delta T \approx \pm$ 10 mK and are contained in the graphic dot size.

To perform the device calibration, we interpolated the smooth $R-T$ dependence of Figure 8 with the following equation

$$\ln R\ (\Omega) = \sum_n C_n[\ln\ T\ (\text{K})]^n \qquad (1)$$

that describes the empirical behavior of a carbon resistor,[38] effective in the range from 4.2 to 300 K. The coefficients of the fit are listed in Table 1.

Table 1. Series Coefficients of the Fit of Eq 1

C_0	C_1	C_2	C_3	C_4
4.1905	0.2347	−0.1175	0.02426	−0.001926

In the whole temperature range, this curve converts the measurement of a resistance value in a temperature value. Because of the smooth behavior, it can be easily used to calibrate the thermometer response. Moreover, the simple interpolation allows minimizes errors, thus improving the accuracy of the measurement. From the $R-T$ behavior shown in Figure 6, we may also evaluate the dimensionless temperature sensitivity that gives the relative change in the sensor output, e.g., the resistance value corresponding to a given relative temperature variation.

$$S = (\text{d}R/R)/(\text{d}T/T) \text{ or } |(\text{d}\ln R)/(\text{d}\ln T)| \qquad (2)$$

In Figure 9, we compare the relative sensitivity of the device (blue curve) with that of commercial thermometers.[36]

Data confirm that the sensitivity of the graphitic microthermometer is slightly lower than bulk commercial thermom-
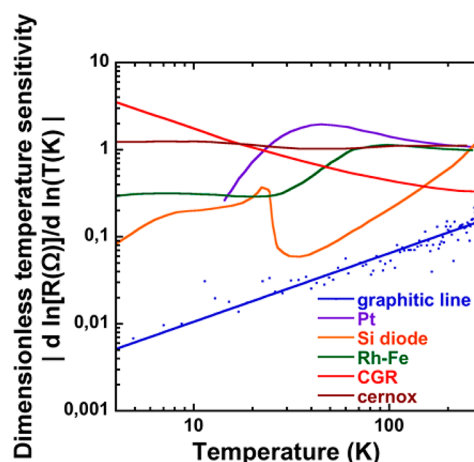

Figure 9. Comparison of the dimensionless temperature sensitivity vs temperature among the graphitic line (blue) and commercial thermometers.

eters over the whole temperature range, although increasing the temperature also increases the sensitivity. The variation is smooth over the entire range from 5×10^{-3} up to 0.2. A typical value[37] for the dimensionless sensitivity is ≥ 0.1, but accuracy and precision are competitive parameters. Summarizing, this "thermometer" exhibits high precision (or reproducibility) in the 4.2−300 K range (see Figure 6), taking into account that this "pattern" has not been designed as a "thermometer". Concerning the resolution ($\Delta T/T$) or the smallest measurable relative temperature variation, we underline that the experimental conditions we used were not optimized for this purpose. The temperature resolution is referred to a Si-diode thermometer used in the experimental setup, and in fact, the voltage measured on the graphitic line resistance is one order of magnitude higher than the typical operating condition (2 mV). Despite this, reasonable values of the normalized temperature resolution are obtained in the entire temperature range and are listed in Table 2 (see also Supporting Information Figure S11). Long-term stability tests performed for different temperature cycles were also successfully carried out.

Table 2. Normalized Temperature Resolution at Different Temperatures

T (K)	4.48	50.9	160.53	298
$\Delta T/T$	0.04	0.02	0.001	0.0009

The graphitic line patterned on the CVD diamond substrate exhibits suitable values of resistance in a wide temperature range (4.2−300 K), lower than MΩ but also not too low (i.e., $\mu\Omega$), a smooth calibration curve, an optimal reproducibility, and suitable values of dimensionless sensitivity and resolution. All are important parameters to design a reliable integrated cryogenic thermometer. Accuracy, a significant feature of a thermometer that indicates how close the measured value is to the true value, is limited by both sensitivity and resolution of the sensor.[37] If a sensor exhibits high sensitivity, then a minor precision in the measuring system is required to achieve a given level of accuracy. In addition, a high-sensitivity sensor works only in a narrow temperature range. The device we realized and tested fulfills all the main figures of a thermometer: it is reproducible in a wide temperature range, it has a smooth calibration curve, and considering sensitivity and resolution, it

exhibits also a good accuracy. For practical applications, it is of great interest that all components of the experimental layout, such as the sample and the thermometer, are in isothermal condition and temperature gradients are negligible. Indeed, another significant feature of a thermometer is the thermal response versus time. Actually, this characteristic is correlated to the size and the packaging of the thermal sensor and a simple thin-film sensor in contact with the sample may certainly guarantee a short thermal response.[37] This patterned device fulfills both the isothermal condition and the thermal response. Being integrated with the diamond substrate, it also shows a good stability during thermal cycles and a fast response. Therefore, the prototype demonstrates that a similar customized compact temperature sensors can be successfully used in many challenging applications, such as temperature measurements inside a DAC cell, now performed with the laser ruby fluorescence.

Heating Tests. In this section we will discuss the performance of compact local microheaters based on such patterned structures. A microheater integrated near a patterned thermometer on a diamond plate, both made with the same fabrication process, is a challenging—but technically feasible—design, suitable to control and characterize a compact setup such as a DAC. The electrical current through the resistive graphitic line may indeed regulate the generated heat. For applications where the heating cycle requires the highest precision, a carbon-based resistive device is probably not the best choice because its resistance changes versus temperature. Indeed, a systematic error occurs because with increasing the temperature a carbon material generates less heat than expected. The sensitivity of our device in the 4.2−300 K temperature range is not high. However, a compact graphitic line patterned on a synthetic diamond, a material with a high thermal conductivity, generates an amount of heat not sufficient to modify its resistance but capable to tune the temperature of the substrate. To characterize the heating behavior, we performed three sets of measurements at $T \approx 4.2$, 83.3, and 293 K. The values of resistance, electric current, and power obtained at different temperatures are listed in Tables 3−5. For

Table 3. Current versus Input Power ($R = 78.661 \pm 0.020$ Ω; $T = 4.20 \pm 0.01$ K)

current ($\Delta I \approx \pm 1~\mu A$)	power ($\Delta W \approx \pm 1~\mu W$)
621 μA	30.3 μW
1.24 mA	120 μW
2.49 mA	487 μW
3.093 mA	751 μW
4.34 mA	1.48 mW
6.27 mA	3.08 mW
8.773 mA	6.04 mW
10.654 mA	8.91 mW

Table 4. Current versus Input Power ($R = 73.758 \pm 0.020$ Ω; $T = 83.35 \pm 0.01$ K)

current ($\Delta I \approx 1~\mu A$)	power ($\Delta W \approx 1~\mu W$)
621 μA	28.42 μW
3.093	705.06 μW
4.24	1.38 mW
6.27	2.89 mW
8.773	5.67 mW
10.654	8.36 mW

Table 5. Current versus Input Power ($R = 65.321 \pm 0.020$ Ω; $T = 290.00 \pm 0.01$ K)

current ($\Delta I \approx 1~\mu A$)	power ($\Delta W \approx 1~\mu W$)
621 μA	25.19 μW
1.85 mA	1223 μW
4.34 mA	1.23 mW
9.41 mA	5.78 mW
12.34 mA	1.48 mW
6.54 mA	10.27 mW
18.81 mA	23.11 mW

heating applications, the thermal response is an important issue. To control the temperature variations of the device versus time, we measured the temperature response, stepwise increasing the applied power.

In Figure 10, we show data collected at $T \approx 4.2$, 83.3, and 290 K (panels A, B, and C, respectively). At the highest temperatures of the thermal bath during the warming up to the plateau temperature, the response of the device exhibits an exponential behavior. At each step of the applied power, the time response of the sample changes, and because of the excellent thermal contact with the heat sink in the liquid helium bath and also to the heat capacity of a material, increasing the temperature to around $T = 4.2$ K (panel A in Figure 10) causes the time response to become really fast. Once the thermal equilibrium between the device and the thermal bath is achieved, a plateau with negligible thermal fluctuations can be observed. Although the system shows a different response versus temperature, the general behavior is excellent as well as the temperature stability, one of the most important characteristics of a heating device.[9]

We also measured the input power vs the temperature of the diamond substrate. It shows a simple linear trend (see the three panels in Figure 11). This result points out that temperature control is feasible and that a linear extrapolation is also possible, a condition particularly appealing for applications where fine-tuning is required.

■ CONCLUSIONS

Many applications and experimental layouts require micro-devices capable of probing and/or finely tuning the temperature. Reliable temperature sensors of micrometric size are still lacking; in addition, reproducible and easy-to-use customizable temperature sensors/devices are not yet available. Advanced instrumentation in thermometry is also fundamental to probe nanoscale heat-transfer phenomena[39] such as phonon transport in nanosystems, molecular thermal transport, etc.

In this study, we showed how it is possible to produce graphitic patterns on thick CVD diamond plates by using a high-power laser. Any geometry is feasible with variable lengths from a few micrometers to several millimeters. Actually, these patterns on diamond might represent a unique solution for thermometry and heating applications. By vibrational spectroscopy and electric transport technique versus temperature, we showed that these patterned structures include well-connected graphitic phases that behave as carbon resistors. We also reported how these low-cost devices, manufactured on synthetic diamond plates, might be used as both thermometer sensors or extremely compact integrated heating devices in experimental layouts such as diamond anvils for high-pressure experiments or cryostats for low-temperature experiments such as those used to characterize superconducting materials.
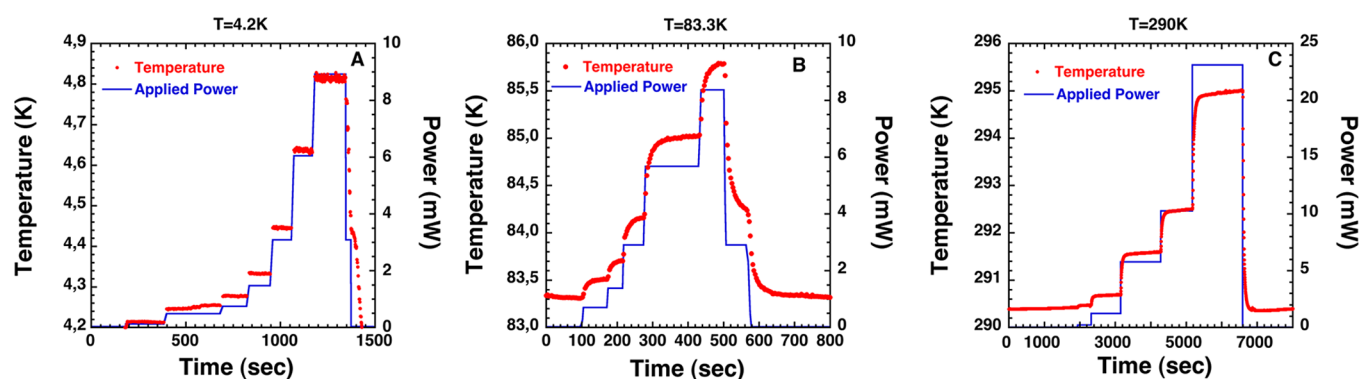
Figure 10. Temperature dependence vs time (red) of the graphitic patterned line measured in a thermal bath at (A) 4.2, (B) 83.3, and (C) 290 K (right) vs the applied power (blue). Error bars are $\Delta T \approx \pm 1$ 0mK and $\Delta W \approx \pm 1$ μW.
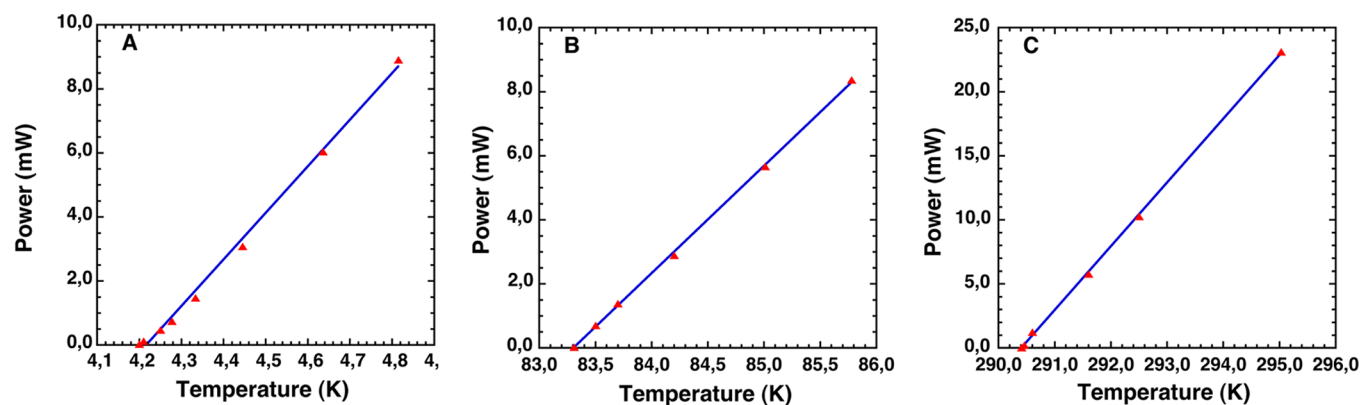

Figure 11. Linear behavior of temperature vs power for different temperatures of the thermal bath: (A) 4.2, (B) 83.3, and (C) 290 K (right). Error bars are $\Delta T \approx 10$ mK and $\Delta W \approx 1$ μW.

However, many other applications are possible in materials science, electronics, micro mechanics, aerospace, biology, etc. Carbon-based structures or films made on diamond surfaces are also suitable sensors for specific technological applications in chemistry, biology, and medicine.[40,41]

The results presented in this contribution demonstrate that a graphitic-patterned device with a total length of 5 mm, width ~30 μm, and depth ~100 μm exhibits a high reproducibility in the temperature range of 4.2−300 K and a smooth calibration equation. Considering its sensitivity (from 5×10^{-3} up to 0.2) and resolution (~1 mK), the accuracy is another interesting feature. Moreover, a similar pattern can be manufactured and customized to become a compact heating device. The performed tests point out a linear behavior with a stable thermal plateau that make possible a reliable control of the temperature versus the input power. The observed linear relationship between power and temperature also guarantees an easy control of the temperature ramp in a wide range, a particularly useful characteristic in many applications. Finally, the microthermometer and microheating system integrated on the diamond plate show a natural isothermal condition and a fast thermal response, two fundamental conditions to have simultaneously all components in a unique, ideal, and compact setup: sample, heater, and thermometer.

ASSOCIATED CONTENT

Ⓢ Supporting Information

Photos of different graphitic pattern produced by laser irradiation on CVD diamond plates, SEM images showing details of patterns, detailed Raman analysis of different points of the pattern, plot showing different rate (K/sec) setups used for resistance versus temperature characterizations, IR measurements at different point of graphitic pattern, and temperature resolution plot comparison of the graphitic pattern and commercial thermometer. The Supporting Information is available free of charge on the ACS Publications website at DOI: 10.1021/acsami.5b02094.

AUTHOR INFORMATION

Corresponding Author

*E-mail: daniele.digioacchino@lnf.infn.it.

Present Address

A.P.: High Field Magnet Laboratory, Institute of Molecules and Materials, Radboud University Nijmegen, Toernooiveld 7, 6525 ED Nijmegen, The Netherlands.

Notes

The authors declare no competing financial interest.

■ REFERENCES

(1) Cahill, D. G.; Goodson, K.; Majumdar, A. Thermometry and Thermal Transport in Micro/Nanoscale Solid-State Devices and Structures. *J. Heat Transfer* **2002**, *124*, 223−241.

(2) Cui, J. B.; Amtmann, K.; Ristein, J.; Ley, L. Noncontact Temperature Measurements of Diamond by Raman Scattering Spectroscopy. *J. Appl. Phys.* **1998**, *83*, 7929−7933.

(3) Weir, S. T.; Jackson, D. D.; Falabella, S.; Samudrala, G.; Vohora, Y. K. An Electrical Microheater Technique for High-Pressure and High-Temperature Diamond Anvil Cell Experiments. *Rev. Sci. Instrum.* **2009**, *80*, 013905.

(4) Ming, L. C.; Basset, W. A. Laser Heating in the Diamond Anvil Press up to 2000° C Sustained and 3000° C Pulsed at Pressures up to 260 kilobars. *Rev. Sci. Instrum.* **1974**, *45*, 1115−1118.

(5) Ishizuka, M.; Amaya, K.; Endo, S. Precise Magnetization Measurements under High Pressures in the Diamond-Anvil Cell. *Rev. Sci. Instrum.* **1995**, *66*, 3307−3310.

(6) Timofeev, Y.; Struzhkin, V. V.; Hemley, R. J.; Mao, H. K.; Gregoryanz, E. A. Improved Techniques for Measurement of Superconductivity in Diamond Anvil Cells by Magnetic Susceptibility. *Rev. Sci. Instrum.* **2002**, *73*, 371−377.

(7) Di Gioacchino, D.; Tripodi, P.; Marcelli, A.; Cestelli Guidi, M.; Piccinini, M.; Postorino, P.; Di Castro, D.; Arcangeletti, E. PRESS-MAG-O: A New Facility to Probe Materials and Phenomena under Extreme Conditions. *J. Phys. Chem. Solids* **2008**, *69*, 2213−2216.

(8) Di Gioacchino, D.; Marcelli, A.; Cestelli Guidi, M.; Piccinini, M.; Puri, A.; Postorino, P.; Pace, E.; De Sio, A.; Gambicorti, L. Status of PRESS-MAG-O: The Experimental Apparatus to Probe Materials and Phenomena under Extreme Conditions at Frascati. *J. Phys. Chem. Solids* **2010**, *71*, 1042−1045.

(9) Zha, C. S.; Basset, W. A. Internal resistive heating in diamond anvil cell for in situ X-ray diffraction and raman scattering. *Rev. Sci. Instrum.* **2003**, *74*, 1255−1262.

(10) Shen, G.; Rivers, M. L.; Wang, Y.; Sutton, S. R. A laser heated diamond cell system at the advanced photon source for in Situ X-ray measurements at high pressure and temperature. *Rev. Sci. Instrum.* **2001**, *72*, 1273−1282.

(11) Shinoda, K.; Nouguchi, N. An Induction Heating Diamond Anvil Cell for High Pressure and Temperature Micro-Raman Spectroscopic Measurements. *Rev. Sci. Instrum.* **2008**, *79*, 015101.

(12) Liu, L.; Basset, W. A. The Melting of Iron to 200 kbar. *J. Geophys. Res.* **1975**, *80*, 3777−3782.

(13) Courts, S. S.; Holmes, D. S.; Swinehart, P. R.; Doddrill, B. C. Cryogenic Thermometry-an Overview. *Appl. Cryog. Technol.* **1991**, *10*, 55−99.

(14) Smedley, J.; Jaye, C.; Bohon, J.; Rao, T.; Fisher, D. Laser Patterning of Diamond. Part I. Characterization of Surface Morphology. *J. Appl. Phys.* **2009**, *105*, 123107.

(15) De Sio, A.; Achard, J.; Tallaire, A.; Sussmann, R. S.; Collins, A. T.; Silva, F.; Pace, E. Electro-Optical Response of a Single-Crystal Diamond Ultraviolet Photoconductor in Transverse Configuration. *Appl. Phys. Lett.* **2005**, *86*, 213504.

(16) De Sio, A.; Bocci, A.; Bruno, P.; Di Benedetto, R.; Greco, V.; Gullotta, G.; Marinelli, M.; Pace, E.; Rubulotta, D.; Scuderi, S.; Verona-Rinati, G. Towards UV Imaging Sensors based on Single-Crystal Diamond Chips for Spectroscopic Applications. *Nucl. Instrum. Methods Phys. Res., Sect. A* **2007**, *583*, 125−130.

(17) Sussmann, R. S., Ed. *CVD Diamond for Electronic Devices and Sensors*; Wiley: Chichester, U.K., 2009.

(18) Morse, J.; Salomé, M.; Berdermann, E.; Pomorski, M.; Cunninghamc, W.; Grant, J. Single Crystal CVD Diamond as an X-ray Beam Monitor. *Diamond Relat. Mater.* **2007**, *16*, S1049−S1052.

(19) Jayaraman, A. Diamond Anvil Cell and High-Pressure Physical Investigations. *Rev. Mod. Phys.* **1983**, *55*, 65−108.

(20) Struzhkin, V.; Hemley, R. J.; Mao, H. K. New Condensed Matter Probes for Diamond Anvil Cell Technology. *J. Phys.: Condens. Matter* **2004**, *16*, S1071−S1086.

(21) Shuker, P.; Melchior, A.; Assor, Y.; Belker, D.; Sterer, E. IR Pyrometry in Diamond Anvil Cell above 400 K. *Rev. Sci. Instrum.* **2008**, *79*, 073908.

(22) Prawer, S.; Nemanich, R. J. Raman Spectroscopy of Diamond and Doped Diamond. *Philos. Trans. R. Soc., A* **2004**, *362*, 2537−2565.

(23) Gondé, C.; Bureau, H.; Burchard, M.; Henry, S.; Simon, G.; Meijer, J.; Kubsky, S. In Situ Temperature Measurements through I-Anvils in Diamond Anvil Cells. *Rev. Sci. Instrum.* **2010**, *81*, 023902.

(24) Zaitsev, A. M.; Dobrinets, I. A. Carbon Nanodots made on Diamond Surface by Focused Ion Beam. *Phys. Status Solidi A* **2005**, *202*, R116−R118.

(25) Zaitsev, A. M. Carbon Nanowires made on Diamond Surface by Focused Ion Beam. *Phys. Status Solidi A* **2006**, *203*, R35−R37.

(26) Pea, M.; Giovine, E.; Di Gioacchino, D.; Marcelli, A.; Della Ventura, G.; Pace, E.; Notargiacomo, A. Morphological and Electrical Characterization of FIB Implanted Diamond Surfaces. *Microelectron. Eng.* **2015**, *141*, 27−31.

(27) Robertson, J. Diamond-like Amorphous Carbon. *Mater. Sci. Eng.* **2002**, *37*, 129−281.

(28) Füner, M.; Wild, C.; Koidl, P. Novel Microwave Plasma Reactor for Diamond Synthesis. *Appl. Phys. Lett.* **1998**, *72*, 1149−1151.

(29) Worner, E.; Wild, C.; Muller-Sebert, W.; Grimm, M.; Koidl, P. High Temperature Infrared Absorption of CVD Diamond Measured by Laser Calorimetry. *Diamond Relat. Mater.* **2005**, *14*, 580−583.

(30) Worner, E.; Wild, C.; Muller-Sebert, W.; Locher, R.; Koidl, P. Thermal Conductivity of CVD diamond films: High-Precision, Temperature-Resolved Measurements. *Diamond Relat. Mater.* **1996**, *5*, 688−692.

(31) Zaitsev, A. M. *Optical Properties of Diamond: A Data Handbook*; Springer: New York, 2001; p 395.

(32) Cestelli Guidi, M.; Piccinini, M.; Marcelli, A.; Nucara, A.; Calvani, P.; Burattini, E. Optical Performance of SINBAD, the IR Source at DAΦNE. *J. Opt. Soc. Am. A* **2005**, *22*, 2810−2817.

(33) Postorino, P.; Congeduti, A.; Degiorgi, E.; Itie, J. P.; Munsch, P. High-pressure behavior of $La_xSr_{2-x}MnO_4$ layered manganites investigated by raman spectroscopy and x-ray diffraction. *Phys. Rev. B* **2002**, *65*, 224102.

(34) Wang, S.; Wu, Z.; Marcelli, A.; Di Gioacchino, D. The AC Multi-Harmonic Magnetic Susceptibility Measurement Setup at the LNF-INFN. *Appl. Mech. Mater.* **2014**, *568−570*, 82−89.

(35) Chalker, P. R. Characterization of Diamond and Diamond-like Films. In *Diamond and Diamond-like Films and Coatings*; Clausing, R. E., Horton, L. L., Angus, J. C., Koidl, P., Eds.; NATO Advanced Study Institute Series B, Vol. *226*; Plenum Press; New York, 1991; pp 127−150.

(36) Chu, P. K.; Li, L. Characterization of Amorphous and Nanocrystalline Carbon Films. *Mater. Chem. Phys.* **2006**, *96*, 253−277.

(37) Ekin, J. W. *Experimental Techniques for Low-Temperature Measurements*; Oxford University Press: Oxford, U.K., 2006; p 189.

(38) Working Group 2 of the Comité Consultatif de Thermométrie *Techniques for Approximating the International Temperature Scale of 1990*; Bureau International des Poids et Mesures: Sèvres, France, 1997; p 108.

(39) Zheng, J.; Wingert, M. C.; Dechaumphai, E.; Chen, R. Sub-Picowatt/Kelvin Resistive Thermometry for Probing Nanoscale Thermal Transport. *Rev. Sci. Instrum.* **2013**, *84*, 114901.

(40) Zaitsev, A. M.; Levine, A. M.; Zaidi, S. H. Carbon Nanowire-Based Temperature Sensor. *Phys. Status Solidi A* **2007**, *204*, 3574−3579.

(41) Kumar, V.; Bergman, A. A.; Gorokhovsky, A. A.; Zaitsev, A. M. Formation of Carbon Nanofilms on Diamond for All-Carbon Based Temperature and Chemical Sensor Application. *Carbon* **2011**, *49*, 1385−1394.